Macroscopic model for development of orientation and ocular dominance columns

Darren M. Pierre and Mehran Kardar
Physics Department, Massachusetts Institute of Technology
Cambridge, Massachusetts 02139, USA
(January 23, 1998)

We develop a *macroscopic* model of the coordinated evolution of ocular dominance and orientation columns in the mammalian visual cortex. Macroscopic approaches have been quite successful in describing patterns formed in many physical systems, in particular following symmetry breaking phase transitions. Ocular dominance, at a coarse-grained scale of many neurons, is modelled by a scalar field, while orientation is represented by a complex number to reflect both its preference and selectivity. Starting with initial conditions of small random fluctuations in the two fields, their time development is assumed to follow from minimization of a cost function. The cost function is only constrained by *analyticity*, *symmetry*, and the requirement of reproducing the *continuity* and *diversity* of the observed patterns. Domain walls in the ocular dominance patterns, and pinwheels in orientation preference, naturally emerge as the defects in the corresponding fields. We pay particular attention to the observed stability of these patterns in the adult response, and to the correlation between the defects. Both observations can be reproduced by including a local coupling between the two fields. It is tempting to rationalize this coupling as a result of the limited computational capacity of the cortex, and the conflicting requirements placed upon it by ocular dominance and orientation preference. Given the possibility of other unknown features in the response, we consider weak coupling to additional fields competing for the above postulated limited computational capacity. Such fields act as sources of randomness, broadening the distribution functions for selectivity and dominance, and may also account for the presence of stable orientation patterns in animals which do not have detectable ocular dominance bands.

I. INTRODUCTION

The preferential response of cells in the primary visual cortex of primates and other mammals to simulations from one eye (ocular dominance), or to lines of a particular direction (orientation selectivity), has been observed for almost half a century. [1] On the larger scale of the whole cortex, the patterns of response are organized into intricate 2-dimensional structures. In 1975 LeVay mapped ocular dominance over most of the primary visual cortex of the macaque monkey using anatomical techniques [2], finding a pattern of wandering and branching bands. Roughly, ten years later, patterns of orientation pinwheels were first recorded by optical imaging. [3]

More specifically, the patterns of response in the macaque monkey have the following features: Ocular dominance is organized in a pattern of alternating wandering and branching bands, whose width fluctuates between 0.4 to 0.5 mm. There are roughly 0.04 branches in an area the size of the square of the branch width. [2] The bands tend to intersect the boundary of the primary visual cortex perpendicularly. Away from the boundary they mostly run toward the calcarine fissure, at least in the top operculum. The transition regions from one eye to the next (domain walls) are sharp in layer 4, and more gradual in the other layers. During post-natal development, the cortex grows by roughly 16%, entirely perpendicularly to the bands. [4] Binocular deprivation has little or no effect on development, while monocular deprivation during a critical period of early development causes the bands corresponding to the deprived eye to shrink while the other bands grow. After the critical period, monocular deprivation has little effect.

A prominent feature of the orientation selectivity pattern are *pinwheels*, areas that respond similarly to all orientations. [3] Different possible orientation preferences circulate around these singularities. The two possible directions of circulation give two types of pinwheels which occur in equal numbers. The density of pinwheels remains constant during the later parts of the critical period (the only observable period of development), despite the growth of the cortex. [5]

Many physical systems exhibit patterns similar to ocular dominance and orientation preference. For example, as temperature is lowered many binary alloys decompose into regions rich in each of the constituent metals. [6] These regions are analogous to the areas in the cortex preferring one eye or the other. In a similar vein, type II superconductors in a magnetic field form vortices which resemble the pinwheels in orientation preference. [7] In both systems the patterns are *macroscopic*, occurring at length scales much larger than those of their (atomic) components. Understanding the emergence of such macroscopic behavior from the interactions of microscopic constituents is the challenge of statistical mechanics.

A. Macroscopic modeling

It is tempting (and natural) to model the formation of patterns, starting with equations describing the coupled behavior of the basic elements: neurons and synapses in the cortex, or the atoms in a binary mixture. However, when most features of interest in the pattern occur at much larger scales, this approach entails a huge cost in following many irrelevant degrees of freedom, and is also subject to uncertainties about the precise behavior of the microscopic degrees of freedom. Fortunately, macroscopic behavior is usually quite robust and independent of microscopic details.

While, many microscopic models can thus "successfully" reproduce the required behavior, it is important to know which features are generic to all models. The macroscopic approach, originally developed in the context of phase transitions by Landau and Ginzburg [8–11], provides the answer. Macroscopic modeling starts by *coarse graining* the system to a length scale intermediate between the microscopic size of the elements, and the longer lengths where collective behavior occurs. The system is then described by a few *collective fields*, or *order parameters*, which encode the average behavior of the elements at the shorter scales, and which fluctuate at longer scales. For example, we shall describe ocular dominance by a scalar field $m(\vec{x})$, and orientation preference by a complex field $z(\vec{x})$, where $\vec{x}$ indicates a position on the (two-dimensional) cortex.

The next step is to construct equations governing the fields based on general ideas such as symmetry and stability, and depending on (hopefully a few) phenomenological parameters. The power of the approach is that because of its generality, and avoidance of microscopic details, it can describe a myriad of situations by simply changing parameters. Its weakness is that, the values of these parameters are not known a priori, and must be obtained by fitting the experimental situation.

B. Cost Function

In many physical systems, the evolution of the order parameter with time t, is governed by an underlying *cost function*. Let us denote the collection of order parameters by $\Psi(\vec{x})$. A particular configuration of the fields entails a cost indicated by the functional $F[\Psi(\vec{x})]$. The simplest possible dynamics is to change the fields so as to minimize the cost [12], by proceeding along the direction of steepest descent in the high dimensional cost "landscape", i.e. $\Psi(\vec{x}, t)$ evolves according to,

$$\frac{\partial \Psi(\vec{x}, t)}{\partial t} = -\mu \frac{\partial F(\Psi)}{\partial \Psi(\vec{x})}, \tag{1}$$

where the "mobility", μ, describes how rapidly the field moves towards a minimum [13]. A system following the above *equation of motion* evolves completely deterministically, and comes to rest at the first *local minimum* where $\partial F/\partial \Psi = 0$. There may be other global minima with lower cost, but the system is prevented from reaching them because it cannot climb out of meta-stable minima.

Given Eq. (1), all the information about the constraints and symmetries of the system must be encoded in the cost function $F[\Psi]$. For example, most systems are *translationally invariant*, i.e. different positions $\vec{x}$ are a priori equivalent. To ensure this invariance, the cost function should not depend explicitly on $\vec{x}$, only implicitly through the order parameter, $\Psi(\vec{x})$, and its derivatives. Many systems are also *rotationally invariant*, prohibiting dependencies such as $\vec{b} \cdot \partial \Psi / \partial \vec{x}$, which explicitly singles out gradients along a particular direction $\vec{b}$. (Externally imposed directions may destroy rotational invariance.)

An important constraint on the macroscopic cost function is *analyticity*. The microscopic variables may well have non-analytic interactions, and response functions, e.g. a heavy-side function is typically used to represent the highly nonlinear response of a single neuron. However, the averaging procedure that leads to the coarse grained fields typically washes out singularities, leading to smooth, analytic behavior. (A well known demonstration is provided by the central limit theorem which that the probability distribution for the average of many random variables, almost always converges to a smooth Gaussian form.) Some existing macroscopic models of the visual cortex use interactions which are not analytic [14–16]. It would indeed be very difficult to justify such non-analyticities at a macroscopic level.

Given the constraint of analyticity, the cost function can be expanded as a power series in Ψ and its gradients, further constrained by the symmetries of the order parameter. For example, due to the a priori equivalence of the two eyes, only even powers of the field $m(\vec{x})$ describing ocular dominance are allowed in $F[m]$. Typically, only a few terms in the power series are sufficient to describe the system; their coefficients are the phenomenological parameters for the problem. For most physical systems the cost function is *local*, in the sense that interactions occur primarily between nearby elements. This implies that the cost function should depend on only a few derivatives of $\Psi(\vec{x})$. (Even the longer range interactions of the so-called "Mexican–hat" form, needed to produce ocular dominance stripes, can be constructed from a second and fourth derivative.)

In the rest of this paper, we apply the macroscopic approach described above to modeling ocular dominance and orientation preference patterns. Since we describe the above features in terms of evolving fields, our model is in several respects similar to other macroscopic models, particularly those by Swindale. [14–16] However, we construct our phenomenological equations by the more general constraints of symmetry and analyticity described above. This approach frees us from becoming entangled in the complexities of modeling individual neurons, which requires dealing with both their great variety and number. It also allows us to apply insights gained from other systems, which have similar symmetries, despite being composed of very different constituents. Models for ocular dominance and orientation preference are developed separately in sections (II) and (III), respectively. The coupling between the two systems is explored in Sec. (IV), and some final observations are presented in Sec. (V).

II. OCULAR DOMINANCE

Ocular dominance at a point $\vec{x}$ can be represented by a real field $m(\vec{x})$. Positive values of m specify one eye, while negative values indicate the other. The strength of the preference is given by the magnitude $|m(\vec{x})|$. In view of the later numerical implementation, we assume a discrete lattice from the outset and label $m(\vec{x}_i)$ with m_i for each lattice point $\vec{x}_i$.

We first examine the *local* parts of the cost function $F(m_i)$, expanded as a power series in m_i. Due to the a priori symmetry between the right and left eyes, the cost should be invariant under interchanging m_i with $-m_i$, thus allowing only even powers of m_i,

$$F(m_i) = a_2 m_i^2 + a_4 m_i^4 + \cdots, \qquad (2)$$

where a_2, a_4, etc. are, as of yet, arbitrary parameters.

We would like the cost function to have its minimum for finite, non-zero values of $|m_i|$, as monocular regions (corresponding to a finite $|m_i|$) are the prevalent feature. Choosing $a_2 < 0$ ensures that $m_i = 0$ is not a minimum, while setting $a_4 > 0$ (and all higher order coefficients zero), results in minimum at a finite value of m_i. It is, of course, possible to meet the requirement for a finite, non-zero minimum in the cost function by many other combinations of higher order terms, but the above simplest choice is generically sufficient.

If we include no interaction between sites, a steepest descent minimization of Eq. (2), results in a set of independent equations of motion for each m_i,

$$\frac{\partial m_i}{\partial t} = -\mu \frac{\partial F(m_i)}{\partial m_i} = -2\mu a_2 m_i - 4\mu a_4 m_i^3. \qquad (3)$$

By appropriate rescalings of m_i and μ, the coefficients a_2 and a_4 can be removed, recasting the above equation into,

$$\tau \frac{\partial m_i}{\partial t} = m_i - m_i^3. \qquad (4)$$

In this form, an unstable fixed point at $m_i = 0$ and stable fixed points at $m_i = \pm 1$ become apparent. In these units, τ is clearly a characteristic relaxation time.

While local terms result in ocular dominance at each point, without further couplings between sites, we cannot generate spatial patterns. The simplest coupling is a nearest neighbor interaction of strength k_s between adjacent sites, leading to

$$\tau \frac{\partial m_i}{\partial t} = m_i - m_i^3 + k_s \sum_{j \,\in\, \text{n.n. } i} (m_j - m_i). \qquad (5)$$

Note that (aside from lattice artifacts), the interactions are *isotropic.* There is some evidence that the growth of the cortex may be anisotropic, but this appears to be a relatively minor effect [5], which we shall ignore. To ensure the continuity of domains, we must choose $k_s > 0$. Thus the absolute minimum of the cost function, its ground state, is a uniform pattern with all $m_i = +1$ or all $m_i = -1$. Thus, there are two degenerate ground states.

We implement these equations numerically, by placing the sites on a discrete hexagonal lattice, and advancing them with finite time steps. (The hexagonal lattice is less anisotropic than the square lattice.) The initial values of m_i were chosen randomly and independently from a distribution centered at 0. We typically used a uniform distribution that allowed m_i to be only a few percent of their saturation value. This distribution is supposed to mimic the initial fluctuations in ocular dominance. Since layer IV is completely enervated by both eyes in the prenatal monkey, it is reasonable to assume that the initial ocular dominance is near zero. The exact distribution is unknown, but has little effect on the simulations.

After a few time constants, a pattern of ocular dominance becomes apparent. The values of $|m_i|$ rise rapidly during this time, saturating to unity. This interval of growth resembles the critical period observed in the monkey. The duration of the interval can be estimated from the linear part of the the equation of motion, as

$$t \approx \tau |\ln |\bar{m}_0||, \qquad (6)$$

and is only weakly dependent on the typical initial magnitude $|\bar{m}_0|$. After this initial period of rapid development, the pattern undergoes smaller changes along the borders between domains, but this *coarsening* occurs on a much longer time.

A. Defects and Coarsening

Iterating Eq. (5) results in a coarse pattern domains of $m_i = \pm 1$ separated by domain walls, as shown in Fig. (1). Each region evolves toward either $m_i = 1$ or $m_i = -1$ depending on the state favored by the random local initial conditions. Since the interactions are of finite range, spatially separated domains can evolve towards different fixed points, resulting in *domain walls.* Domain walls are thus the natural defects in systems with two (or a few) degenerate lowest cost states, and as such quite common. An simple example is provided by a glass of ice water; domain walls between the solid and liquid states of water occur, because at 0°C, the two phases are degenerate in free energy cost.

With only nearest neighbor interactions, m_i changes abruptly at the domain walls. Almost all sites have $|m_i| \approx 1$, which corresponds to completely monocular cells. These domain walls are very similar to the band walls seen in layer 4 of the visual cortex. Unfortunately, nearest neighbor interactions do not generate a regular pattern of bands.

The minimum of the cost function is a state in which all m_i are aligned. Domain walls incur a cost penalty proportional to their length. Thus as time goes on, the system tends to remove and heal these defects, progressing towards a pattern with coarser domains. In our deterministic system coarsening occurs through the shrinking (and eventual disappearance) of smaller islands in larger domains. Unfortunately, an artifact of the discretization causes the pattern to freeze in meta-stable states of high cost, such as in Fig. (1). In a continuous system islands always shrink, as the boundary can be smoothly deformed inward, slowly lowering the cost of the pattern. On the discretized lattice, small islands still shrink and disappear, but islands above a critical size, controlled by k_s, remain. Removing these islands requires temporarily passing over configurations of higher cost, which is not permitted by our equations of motion.

It is tempting to use this effect to stabilize patterns of ocular dominance, but this is not in keeping with the macroscopic approach. It relies on a microscopic feature, the discrete nature of the lattice, to control the macroscopic properties. Even though the actual system is in fact composed of discrete neurons, our coarse grained variables in fact represent many neurons. If we identify each lattice point with a single neuron, we must then model its complicated processing tasks, and couplings to other neurons through tree like arbors of axons and dendrites.

B. Stabilization

Many systems in nature exhibit patterns of stripes; magnets with dipole interactions, zebras, bird feathers, many species of fish, and even fingerprints, are but a few examples. Following the early work by Turing, reaction-diffusion models have been frequently used to model such systems. [17] The common mechanism for generation of stripes, at least in the better understood cases, is a competition between short range attraction and longer range repulsion. In the context of the visual cortex, this idea was first proposed by Hubel and Wiesel in 1977. [18] As the short range and the long range interactions cannot be simultaneously satisfied, the best compromise is a regular arrangement of domains into stripes whose character and width is determined by the interactions. In our deterministic equations, the randomness in the initial conditions provides the seed for the irregular branching and bending of the stripes.

Going beyond nearest neighbors, we generalize Eq. (5) to

$$\tau \frac{\partial m_i}{\partial t} = a m_i - m_i^3 + \sum_j k_{ij}(m_j - m_i), \tag{7}$$

where the interaction matrix k_{ij} depends only on the distance between sites i and j. Specifically, we chose

$$k_{ij} = \begin{cases} k_s & \text{if } i \text{ and } j \text{ are within } L/2 \text{ sites of each other,} \\ k_l & \text{if } i \text{ and } j \text{ are between } L/2+1 \text{ and } L \text{ apart,} \end{cases} \tag{8}$$

where L is the range of the coupling. To ensure the continuity of the domains, $k_s > 0$, while $k_l < 0$ is needed to achieve a periodic alternation in the sign of m_i.

As a technical point we remark that while in the absence of couplings, a positive coefficient for the linear term in the equation of motion ($a > 0$) is necessary to ensure that $m_i = 0$ was not a stable solution, this is not necessary in the presence of couplings. From Eqs. (7) and (8), we note that for a random initial condition $dm_i/dt \approx (a - N_s k_s + N_l |k_l|)$, where N_s and N_l are the number of short- and long-range couplings in Eq. (8) respectively. The negative long-range couplings are thus sufficient to destabilize the $m_i = 0$ fixed point, and we find that using a negative coefficient, $a < 0$, gives better results.

1. *Bands and Their Width*

The long range interactions result in a pattern of bands with a width of slightly less than $2L$, as shown in Fig. (2). The width can be estimated by looking at the Fourier transform of the interaction. A peak in the Fourier spectrum indicates a period selected by the interactions. The Fourier spectrum of Eq. (8) results in a sum of Bessel functions,

$$K(s) = k_s \sum_{l=1}^{L/2} l J_0(2\pi l s) + k_l \sum_{l=L/2+1}^{L} l J_0(l 2\pi l s). \tag{9}$$

For a value of $L = 10$ with $k_s = -k_l$, $K(s)$ has a peak at approximately $s = 0.068$, corresponding to a period of 14.7, consistent with the strip width in the simulations.

Many other interactions with the same typical structure in Fourier space result in a similar pattern of bands. While the functional form in Eq. (9) is rather complicated, its essence can be captured by the much simpler form $K(s) = s^2 - L^2 s^4$. Most interactions with competing positive short range interactions and negative long range interactions have a similar $K(s)$. It is tempting to try to determine the exact shape of the interaction be studying the distribution of excitatory and inhibitory connections on individual cells. However, it is important to distinguish the neural network that mediates the response of visual cortex from the unknown interaction that directs its evolution. The existing connections in the mature animal are certainly responsible for generating the response at a particular location to stimuli. But, as we wish to study the development of these connections, it is necessary to find the neuro or chemical interactions responsible for their initial development.

2. Persistence

Persistence is a measure of the internal order of the stripes which includes the density of branches and the straightness of the bands. Some aspects of persistence, such as the number of branch points, are easy to quantify. For example, the pattern published by LeVay in Ref. [2] has 190 branches, for a density of roughly 0.6 per mm^2, or 0.04 ends per area equal to square of the band width. This latter measure is more useful as the brain undergoes significant shrinkage during LeVay's preparation. The number of branch points, where one band breaks into two, is the same as the number of end points except for corrections at the boundaries.

Measuring the persistence on longer scales, i.e. the straightness of the bands, is more difficult. Typically, when comparing different results or simulations, we are forced to rely on the qualitative appearance. The persistence of the bands in our simulations is determined mainly by the long range interaction strength, increasing with k_l. The short range interaction strength k_s controls the roughness of individual domain walls.

3. Edge Effects

Boundary conditions play an important role in the overall appearance of the patterns. The patterns of Fig. (2) were generated with periodic boundary conditions in which the sites at one edge connect to the opposite edge. Such boundary conditions are frequently used to reduce edge effects. However, to simulate the whole cortex, open boundary conditions may be more appropriate. With open boundary conditions, there are fewer connections for the sites close to edges, as they have fewer neighbors. This more accurately reflects the cells near the edge of the primary visual cortex, which receive a limited amount of ocular dominance information. As we shall demonstrate below, open boundary conditions favor stripes which run orthogonal to the edges. Fig. (3) shows the results of a simulation with open boundary conditions.

The behavior of the stripes at the open edges can be understood by examining the cost function. The absence of interactions at the edge leads to an additional cost penalty compared to an infinite system. This penalty depends on the angle at which the bands intersect the edge. As a simple model, consider a continuous system in which $m(\vec{x})$ abruptly switches from +1 to -1 in alternating bands of width L. The extra cost associated with missing bonds (or range L) at the edge is calculated from

$$\Delta F = \int d^2x d^2x' m(\vec{x}) m(\vec{x}') \delta(|x - x'| - L). \qquad (10)$$

The edge is an open boundary with $m(\vec{x}) = 0$ on the far side. The final cost of this edge per unit length of the boundary is given by,

$$\Delta F_{\text{edge}} = 2L^2 \left(\cos(\theta) - 1 + \theta \sin(\theta)\right). \qquad (11)$$

This function, shown in Fig. (4), has a minimum at $\theta = 0$, corresponding to stripes perpendicular to the edge. We also performed the calculation on a hexagonal lattice with stripes of width 10 lattice points. The discrete and continuous calculations are compared in Fig. (4). While small differences occur, the general angular dependence is similar in the two cases.

4. Monocular Deprivation

In monocular deprivation experiments, one eye is closed or otherwise inhibited during part of development. If this occurs during the critical period of early development, ocular dominance begins to favor the open eye. We can model monocular deprivation by adding a bias to the equation of motion, as

$$\tau \frac{\partial m_i}{\partial t} = a m_i - m_i^3 + \sum_j k_{ij}(m_j - m_i) + H(t), \qquad (12)$$

where $H(t)$ mimics the strength of the preference caused by monocular deprivation, which could in principle depend on time. I n the Landau-Ginzburg language, $H(t)$ is a *symmetry breaking field* that prefers one eye.

Such symmetry breaking reproduces some features of monocular deprivation. If the field is applied early in the simulation, it results in a preference for one eye over the other, while if applied in the later stages, it has little or no effect. Like monocular deprivation, it is effective only during a critical period. However, it does not reproduce the observed pattern of alternating narrow and wide bands. Instead, a pattern forms with islands of the deprived eye appearing in a sea of the dominate eye. The typical width of features for both eyes remains constant, while the overall area covered by the deprived eye is reduced by an amount depending on the $|H(t)|$. For sufficiently large values of $|H(t)|$, the symmetry breaking field dominates and a uniform pattern results.

III. ORIENTATION PREFERENCE AND SELECTIVITY

We use a complex field, z_i, to model orientation preference and selectivity. The orientation preference is given by half of the complex angle, since it repeats with a period of 180°. The magnitude of the complex field, $|z_i|$, is a measure of the selectivity.

We construct a local cost function $F(z_i)$ by considerations similar to those in Sec. (II). Because there is no a priori reason to distinguish between different orientations, the cortical cost function must be only a function of the absolute value, $|z_i|$. However, odd powers of $|z_i|$ are not analytic (smooth) around $z_i = 0$, and will not be included in the cost function. The local part of the cost is therefore expanded as,

$$F(z_i) = a_2'|z_i|^2 + a_4'|z_i|^4 + \cdots, \tag{13}$$

where a_2', a_4', etc. are again arbitrary parameters.

As in our model for ocular dominance, choosing $a_2' < 0$ and $a_4' > 0$, and setting all other coefficients zero, results in a minimum cost for a finite $|z_i|$. A steepest descent minimization of this local cost function gives an independent equation of motion for each z_i,

$$\frac{\partial z_i}{\partial t} = -\mu' \frac{\partial F(z_i)}{\partial z_i} = -2\mu' a_2' z_i - 4\mu' a_4' z_i |z_i|^2. \tag{14}$$

Absorbing the coefficients a_2' and a_4' by appropriate rescalings, results in

$$\tau' \frac{\partial z_i}{\partial t} = z_i - z_i |z_i|^2. \tag{15}$$

There is a continuous set of stable fixed points with $|z_i| = 1$, and τ' is a characteristic time for relaxation. Including isotropic nearest neighbor couplings results in,

$$\tau' \frac{\partial z_i}{\partial t} = z_i - z_i |z_i|^2 + k_s' \sum_{j \,\in\, \mathrm{n.n.}} (z_j - z_i). \tag{16}$$

Again, the coupling strength k_s', between adjacent sites must be positive to ensure the continuity of domains.

The exact distribution of orientation preference and selectivity at early stages of development is not known. A reasonable assumption is a uniform distribution of angles. Experiments also show that selectivity is lower in immature animals. To model this information, we assume initial conditions for z_i that are uniform on the complex angle with a fixed magnitude that is small, typically $|z_i| = 0.1$. (It is likely that the initial magnitude is also distributed over some range, but as there is little information on this, and the final results are not affected, we choose to simply use a single initial value.)

We performed simulations with both periodic and open boundary conditions. Because of the short-range nature of the interactions, boundary conditions do not seem to play a significant role. There is experimental evidence that orientation continues smoothly from area V1 to neighboring area V2, suggesting that open boundary conditions are not necessary.

A. Defects and Coarsening

In a numerical simulation, orientation preference rises quickly in the first several time constants until it approaches a saturation value of approximately unity. This initial interval is a critical period where the field is sensitive to small perturbations. As shown in Fig. (5)a, the resulting pattern is marked by singularities called *vortices*, which are points of reduced selectivity surrounded by regions responding to all possible orientations. These vortices are defects in the pattern, which correspond to the pinwheels observed experimentally.

Vortices are well defined topological features, that can be detected by adding together the changes in angular preference around a closed loop. If this sum is $\pm 180°$, a vortex is enclosed in the loop. The vortex has a circulation of ± 1 depending on sign of the sum. Our simulations give equal numbers of vortices of each circulation, in agreement with experimental observations. Since vortices are the natural defects in angular fields, it is not surprising that they are generated by a wide variety of apparently disparate models. Any model that gives adequate attention to the angular nature of the orientation pattern will generate vortices.

The ground state, the absolute minimum of the cost function, occurs when all sites have the same orientation. Since the cost is independent of the global orientation, this ground state is highly degenerate. Vortices arise because the short-range interactions allow separated regions to relax independently. Each region evolves towards one of these degenerate ground states that is favored locally by the initial conditions. While domain walls are the resulting defects in systems breaking a *discrete* symmetry, they do not occur in systems with *continuous* symmetry, since adjacent "domains" can be smoothly connected by smooth deformations. Vortices, however, are topological defects and cannot be removed by smooth changes.

Vortices of opposite circulation experience an effective attraction. This attraction causes opposite vortices to more toward each other, collide, annihilate in pairs, slowly reducing their overall density, as shown in Fig. (6). In this manner the pattern continues to coarsen and evolve toward the uniform ground state. This takes place on a much longer time scale than the initial formation of vortices. Such coarsening is in sharp contrast to the experimental observations where the vortex concentration remains constant. [5]

B. Stabilization

Long range couplings, which stabilized the pattern of ocular dominance, are not effective for fixing the pattern of orientation preference. We considered a variety of different long range interaction forms consistent with the symmetry of the system. Rather than stabilizing a pattern of vortices, these interactions lead to patterns with rainbow-like "orientation bands" and without vortices.

An effective approach for stopping the motion of vortices is by pinning to impurities. This is an important mechanism for stopping the unwanted motion of vortex lines in superconductors. In the cortex, randomness can arise from fluctuations in the density or effectiveness of the neurons Small fluctuations in neuron density are indeed observed in the cortex, and might reasonably be considered as uncorrelated. Fluctuations in computational effectiveness have not been studied in the monkey, but are a reasonable assumption considering the variety of different types of neurons present.

Quenched randomness that represents density fluctuations is best represented by a set of real numbers $\{h'_i\}$, that modify the equation of motion to

$$\tau' \frac{\partial z_i}{\partial t} = z_i - z_i|z_i|^2 + k'_s \sum_{j \,\in\, \mathrm{n.n.}} (z_j - z_i) + h'_i z_i. \quad (17)$$

If we ignore the couplings between sites, i.e. for

$$\tau' \frac{\partial z_i}{\partial t} = z_i - z_i|z_i|^2 + h'_i z_i, \quad (18)$$

the local variable $|z_i|$ evolves to a fixed magnitude of $\sqrt{1+h'_i}$. This form of randomness thus modifies the local selectivities, without favoring specific orientations.

It is difficult to biologically motivate a particular distribution for $\{h'_i\}$, as we have not specifically identified the processes generating randomness. Summing over many independent processes usually leads to a Gaussian distribution. Randomness arising from structural fluctuations in the cortex may well lead to other distributions. We use a uniform distribution for convenience, but believe that other choices give qualitatively similar results.

Fig. (7)a shows the result of a simulation with randomness. Vortices become trapped, or pinned, in locations where randomness favors small $|z_i|$. A sufficient amount of randomness creates a pattern of vortices that is stable over long time scales. Smaller amounts of randomness slow, but do not prevent, the pair annihilations. Coupling to $\{h'_i\}$ also widens the distribution of $|z_i|$ and may disrupt the overall pattern of selectivity. In the selectivity pattern shown in Fig 7b, vortices are no longer clearly visible, as the variations are largely dominated by randomness. It is possible that inclusion of longer range interactions, which increase the size of vortices, may restore their prominence in the selectivity pattern.

Although we only investigated the effects of *local* randomness, random couplings (modeled by adding random fluctuations δ'_{ij} to k'_{ij}) generate many of the same effects. Random couplings may reflect fluctuations in the ease with which synapses are formed between groups of cells. The size, orientation, and exact position of cells are likely to effect their ability to form synapses with other nearby cells.

IV. COUPLING OCULAR DOMINANCE AND ORIENTATION SELECTIVITY

Coupling between ocular dominance and orientation selectivity can play an important role in establishing the patterns of the two fields. Since orientation singularities have been observed to lie in the center of ocular dominance bands, and lines of iso-orientation meet ocular dominance domain walls perpendicularly, some form of coupling must exist. [19] As we shall demonstrate, such interactions can also stabilize the pattern of pinwheels, and significantly effect the distribution of ocular dominance and selectivity.

Let us first construct a local cost function for both fields. All the terms present in individual cost functions of Eqs. (2) and (13) must be included plus additional interactions. The simplest interaction term which is invariant under $m \to -m$ and independent of the complex angle, is $m_i^2|z_i|^2$. Higher order terms are possible in principle, but not likely to be important in a macroscopic cost function. The resulting local cost function,

$$F(m_i, z_i) = a_2 m_i^2 + a_4 m_i^4 + a'_2|z_i|^2 + a'_4|z_i|^4 + g m_i^2|z_i|^2, \quad (19)$$

has five free parameters a_2, a_4, a'_2, a'_4, and g. The corresponding equations motion,

$$\frac{1}{\mu}\frac{\partial m_i}{\partial t} = -2a_2 m_i - 4a_4 m_i^3 - 2g m_i|z_i|^2, \quad (20)$$

$$\frac{1}{\mu'}\frac{\partial z_i}{\partial t} = -2a'_2 z_i - 4a'_4 z_i|z_i|^2 - 2g z_i m_i^2, \quad (21)$$

also depend on two mobility parameters μ and μ' . To ensure finite fixed points, a_2 and a'_2 must be negative while a_4 and a'_4 are positive. By appropriately rescalings, we can reduce the local equations to

$$\tau \frac{\partial m_i}{\partial t} = m_i - m_i^3 - \gamma m_i|z_i|^2,$$
$$\tau' \frac{\partial z_i}{\partial t} = z_i - z_i|z_i|^2 - \gamma' z_i m_i^2, \quad (22)$$

where $\gamma' = a'_4/a_4\gamma$, and τ and τ' are time constants. The couplings, γ and γ', do not have to be equal but must have the same sign. (Eqs. (22) can be rewritten with identical coefficients for the coupling terms but different coefficients on the linear and cubic terms.)

We next couple the sites through the interactions developed in the previous sections. The full equations of motion,

$$\tau \frac{\partial m_i}{\partial t} = -m_i - m_i^3 - \gamma m_i|z_i|^2 + \sum_j k(i,j)(m_j - m_i),$$
$$\tau' \frac{\partial z_i}{\partial t} = z_i - z_i|z_i|^2 - \gamma' z_i m_i^2 + k'_s \sum_{j \,\in\, \mathrm{n.n.}} (z_j - z_i), \quad (23)$$

contain 5 parameters in addition to the interaction k_{ij}. Setting $\tau = 1$, τ' should be determined by comparing the growth rate of orientation preference to ocular dominance. Unfortunately, there is currently not enough data on immature animals to compare the two rates, and we set $\tau' = \tau = 1$. We further assume $\gamma = \gamma'$, as there is no compelling reason for one field to play a dominate role over the other. Note that, once again, we have reversed the sign of m_i, as discussed in Sec. (II B).

A. Defects and Coupling

A small positive value of $\gamma = \gamma' = g$ is enough to cause the vortices to tend to avoid the domain walls, as seen in Fig. (8). The positive term $gm_i^2|z_i|^2$ in the cost function of Eq. (19), implies that sites with both high ocular dominance and orientation selectivity incur an additional cost. Defects in either field, which have low values of m_i or z_i, can reduce the total cost by appearing at separate sites, so as to save a cost proportional to g. (The existence of defects still adds to the total cost.) The presence of orientation vortices in the center of ocular dominance bands in turn leads to iso-orientation lines which cross ocular dominance domain walls perpendicularly.

The quartic terms in the local cost function of Eq. (19) can be combined into a form proportional to $(m_i^2 + \tilde{g}|z_i|^2)^2$, where g, $\tilde{g}$, γ, and γ' all have the same sign. The cost function is now extremized when the combination $m_i^2 + \tilde{g}|z_i|^2$ saturates to a fixed value of the order of unity. Clearly, a positive g describes a *competition* between ocular dominance and orientation for a share of this fixed value. For negative values of g, on the other hand, $|m_i|$ and $|z_i|$ can grow in concert. In this case vortices preferentially line up on the ocular dominance domain walls. The latter pattern, however, is not seen experimentally.

Large positive values of γ distort the pattern of orientation and ocular dominance. The cortex becomes divided into region responding only to orientation or only to ocular dominance. Across the centers of ocular dominance bands orientation becomes discontinuous. This discontinuity is similar to the fractures seem experimentally. However, for these large couplings, fractures, rather than pinwheels, are the dominant feature.

B. Stabilization

Coupling between ocular dominance and orientation preference can by itself prevent the coarsening and merging of orientation vortices. A pattern free of vortices still has the globally lowest cost. However, most initial conditions do not evolve to this global minimum. Instead, they become trapped in local minima that still contains vortices. Since vortices are topological defects, they can only be removed by annihilation with opposite vortices (or by escaping through an edge). Due to the coupling (with positive g), the ocular dominance domain walls act as barriers to vortex motion. A vortex onto a domain wall increases the cost of the pattern, and is prohibited from doing so, even though a lower cost may be achieved when the vortex has passed though the domain wall.

The eventual distance between vortices is thus set by the width and persistence of the ocular dominance bands. The width of the bands provides the separation in the direction perpendicular to the stripes, while parallel to the bands, the typical separation of vortices is limited by the persistence. In frequently branching and bending bands, vortices are quickly trapped in the curves. In relatively straight bands, however, considerable rearrangement can occur without becoming entangled in the domain walls.

Two other consequences of the coupling g are worth mentioning. The first is its role on he distributions of the magnitudes $|z|$ and $|m|$: In the absence of randomness, the distributions for the magnitudes are too uniform; except in the vicinity of defects, the magnitudes saturate to the fixed point value. As demonstrated in Fig. (9), the coupling has the desirable feature of widening the distributions. An undesired feature, is the influence on the pattern of selectivity, as shown in Fig. (8)b. Unlike in the experimental case, the ocular dominance domains are visible in the pattern of selectivity. While the strength of this effect varies with the magnitude of γ, it persists even at very small values of the coupling. Coupling to additional fields, or random noise, may disguise the effect from visual observation, but it would still be detectable statistically. No published statistical analysis of experimental data has yet shown any sign of the ocular dominance domain walls in orientation selectivity patterns.

V. CONCLUSIONS

Macroscopic modeling is capable of reproducing many of the patterns observed in the response of the primary visual cortex. This approach is based on the nature and symmetry of the emergent properties of the cortex, and provides insight into the key microscopic features responsible for the global patterns.

Ocular dominance is represented a real field $m(\vec{x})$ that encodes the dominant eye and the degree of preference. The a priori symmetry between the two eyes limits the equations of our model to those unchanged under a global inversion $m(\vec{x}) \to -m(\vec{x})$. Initial conditions, reflecting a nearly binocular response, develop into a pattern of domains of different signs, corresponding to the observed monocular bands. This initial development occurs during a critical period during which the model is very sensitive to perturbations. Different domains are separated by boundaries where $m(\vec{x})$ changes rapidly, as seen in ocular dominance bands in layer 4 of the visual cortex. Competition between short range excitations, which favor continuity, and long range inhibitions, which encourage diversity, stabilizes the domains, and results in this pattern of stripes. Without this competition, the domains coarsen to reduce the extra cost associated with the domain walls, eventually resulting in uniform (monocular) response.

We model orientation by a complex field $z(\vec{x})$ to reflect both angular preference and selectivity strength. The symmetry among orientations limits the model to a few phenomenological terms that are invariant under a global change of phase $z(\vec{x}) \to e^{i\phi} z(\vec{x})$. Random initial conditions evolve under the resulting equations of motion into patterns which contain vortices. Vortices are the natural defect in angular fields, and are naturally associated with the pinwheels observed in the response of the cortex. The simulated preferences are sensitive to small perturbations during a brief initial period. As vortices are costly defects, which tend to slowly annihilate in pairs, some additional factor is needed to stabilize a pattern with a finite density of vortices. We find that coupling to quenched randomness, or to the pattern of ocular dominance, can stabilize the pattern of orientation.

In addition to stabilizing orientation patterns, coupling between the ocular dominance and orientation fields explains the tendencies for pinwheels to avoid the edges of ocular dominance bands. It is natural to think of this coupling as a result of the cortex's limited computational capacity, e.g. areas which respond strongly to orientation have less ability to simultaneously respond strongly to ocular dominance. This coupling relates the typical separation between vortices to the length scales of the ocular dominance domains. This may explain why both features are observed to have very similar length scales. However, we must consider this interpretation with caution. Both orientation and ocular dominance are mediated by neural activity which has an inherent length scale. The size of neural arbors is roughly commensurate with both the band width and the separation between pinwheels.

A. Additional Fields

It is likely that the cortex self-organizes to exhibit preferential local response to a variety of other visual inputs such as color, texture, motion, and so on. Some of these features may rely on similar aspects of information provided by the visual input, such as orientation and direction of motion. Other varieties of response may depend on uncorrelated aspects of the input, as is apparently the case for ocular dominance and orientation. Let us represent the latter proposed independent features by a set of additional fields, which will be collectively denoted by the vector $\Phi(\vec{x})$.

In analogy to the discussions of Sec. (IV), we can construct a local cost function which is minimized when the combination $\left(m_i^2 + |z_i|^2 + \Phi_i \cdot \Phi_i\right)$ (after appropriately rescalings of the magnitudes of the fields) saturates to a finite value (say unity). Being rather careless with numerical coefficients, such a cost function leads to a set of independent equations of motion at each site

$$\begin{aligned} \tau \frac{\partial m_i}{\partial t} &= m_i - m_i \left(m_i^2 + |z_i|^2 + \Phi_i \cdot \Phi_i\right), \\ \tau' \frac{\partial z_i}{\partial t} &= z_i - z_i \left(m_i^2 + |z_i|^2 + \Phi_i \cdot \Phi_i\right), \\ \tau^{(\alpha)} \frac{\partial \Phi_i^{(\alpha)}}{\partial t} &= \Phi_i^{(\alpha)} - \Phi_i^{(\alpha)} \left(m_i^2 + |z_i|^2 + \Phi_i \cdot \Phi_i\right), \end{aligned} \tag{24}$$

where the superscript (α) refers to a particular component of Φ. Note that if some of the time scales $\tau^{(\alpha)}$ are fast, the corresponding fields reach their saturation value rapidly. They then act as a source of randomness on the remaining slow fields. This provides the motivation for the randomness introduced in Sec. (III B).

Coupling to additional fields will further result in the desirable feature of broadening the distributions for ocular dominance and orientation selectivity, bringing them into better conformity with observations. It may also account for the presence of stable orientation patterns in animals which do not have detectable ocular dominance bands. It would be interesting to numerically and experimentally explore the number and types of independent features that are encoded in the cortical response. A particularly interesting challenge is to incorporate topographical maps on the cortex in this macroscopic formalism.

B. Open Questions

Despite the success of macroscopic modeling, several questions remain. The distributions for orientation selectivity and the magnitude of ocular dominance generated by the model, are much sharper than the observed distributions. Limited information is currently available about these distributions; further experimental studies would significantly guide the development of models. The existing data suggests that in layers other than 4, the ocular dominance distribution may be quite wide, including a significant number of binocular cells with low values of $|m_i|$. [18] Our own analysis of optical imaging data in the ferret (obtained in the lab of Prof. M. Sur at MIT [20]) suggests a distribution of selectivity that is wider than those generated by our model. This interpretation is, however, complicated by the steps involved in converting the raw data to values for the selectivity. As many of the other models have not looked explicitly at these distributions (but do not seem to do any better), this an area in need of further study. The distribution of ocular dominance magnitudes reflects the sharpness of the domain walls, and should be correlated to the response to monocular deprivation. Stripes with sharp domain walls are not able to easily narrow or widen under the influence of monocular deprivation as observed in our simulations.

The primary visual cortex grows significantly during the formation of orientation and ocular dominance patterns. We did not model this effect, as simulating growth of the cortex requires adding lattice points during the simulation to reflect the appearance of new cells. Some correlation between growth and ocular dominance is necessary to explain the observed propensity of the growth to be perpendicular to the bands. Modeling growth must also be accompanied by the spontaneous creation of vortex pairs in the orientation pattern, if the pinwheel density does indeed remain constant. Additional experiments that probe the evolution of patterns during development will provide more stringent tests for developmental models than currently available.

More detailed characterization of the observed patterns will greatly help in differentiating between models. Currently, much of the comparison to experiments is simply visual. Measuring correlation functions for various fields, and their defects, allows for more quantitative comparisons than discussions of linear zones, saddle points, fractures, and singularities. Recently Obermayer and Blasdel have begun work in this direction, measuring correlation functions in orientation patterns, and finding that the patterns cannot be entirely reconstructed by the positions of their pinwheels. [21] Further work in this direction will lead to additional quantitative tests for models, hopefully leading to greater insight into the workings of the visual cortex.

ACKNOWLEDGMENTS

We are grateful to Mriganka Sur, Bhavin Sheth, and Jitendra Sharma for introducing us to this problem, and sharing their understanding and data. The comments and guidance of Peter Dayan have been particularly useful. We acknowledge the financial support of the National Science Foundation (through Grant No. DMR-93-03667) and the Office of Naval Research (through the ONR Fellowship Program).

---

[1] David H. Hubel. Evolution of ideas on the primary visual cortex, 1955-1978: A biased historical account. *Bioscience Reports*, 2:435–469, 1982.

[2] Simon LeVay, David H. Hubel, and Torsten N. Wiesel. The pattern of ocular dominance columns in macaque visual cortex revealed by reduced silver stain. *Journal of Comparative Neurology*, 159:559–576, 1975.

[3] Gary G. Blasdel and Guy Salama. Voltage-sensitive dyes reveal a modular organization in the monkey striate cortex. *Nature*, 321:579–585, 1986.

[4] D. Purves and A. LaMantia. Development of blobs in the visual cortex of macaques. *Journal of Comparative Neurology*, 322:1–7, 1993.

[5] Klaus Obermayer and Gary G. Blasdel. Geometry of orientaton and ocular dominance columns in monkey striate cortex. *The Journal of Neuroscience*, 13:4114–4129, 1993.

[6] Kerson Huang. *Statistical Mechanics.* John Wiley & Sons, 1987.

[7] J. R. Schrieffer. *Theory of Superconductivity.* Addison-Wesley Publishing Company, 1983.

[8] L. D. Landau. On the theory of phase transitions. In D. Ter Haar, editor, *Collected Papers of L. D. Landau*, chapter 29, pages 193–216. Gordon and Breach, 1967.

[9] L. D. Landau. On the theory of phase transitions. *Journal of Experimental and Theoretical Physics (Russian Language)*, 11:26, 1937.

[10] V. L. Ginzburg and L. D. Landau. On the theory of superconductivity. In D. Ter Haar, editor, *Collected Papers of L. D. Landau*, chapter 73, pages 546–568. Gordon and Breach, 1967.

[11] V. L. Ginzburg and L. D. Landau. On the theory of superconductivity. *Journal of Experimental and Theoretical Physics (Russian Language)*, 20:1064, 1950.

[12] Note that generating the equation of motion from a cost function leads to certain constraints which may be absent in the non-equilibrium system. For example, this procedure restricts the coupling between sites to be symmetrical (e.g. $k_{ij} = k_{ji}$ in Eq. (7).

[13] Even for a given cost function, the equation of motion is not unique. The steepest gradient descent corresponds to the zero temperature limit of dynamics in a system with no conservation laws, or model A in the notation of P. C. Hohenberg and B. I. Halperin. Theory of dynamic critical phenomena. *Reviews of Modern Physics*, 49:435–479, 1977.

[14] N. V. Swindale. A model for the formation of ocular dominance stripes. *Proceedings of the Royal Society of London, Series B*, 208:243–264, 1980.

[15] N. V. Swindale. A model for the formation of orientation columns. *Proceeding of the Royal Society of London, Series B*, 215:211–230, 1982.

[16] N. V. Swindale. A model for the coordinated development of columnar systems in primate striate cortex. *Biological Cybernetics*, 66:217–230, 1992.

[17] A M Turing. The chemical basis for morphogenesis. *Philisophical Transactions of the Royal Society of London B*, 237:37–72, 1952.

[18] D. H. Hubel and T. N. Wiesel. Functional architecture of macaque monkey visual cortex. *Proceeding of the Royal Society of London, Series B*, 198:1–59, July 1977.

[19] Gary G. Blasdel. Orientation selectivity, preference, and continuity in the monkey striate cortex. *The Journal of Neuroscience*, 12:3139–3161, 1992.

[20] Mirganka Sur. Unpublished data for orientation selectivity and preference in the ferret.

[21] Klaus Obermayer and Gary G. Blasdel. Singularities in primate orientation maps. *Neural Computation*, 9:555–575, 1997.

FIGURES

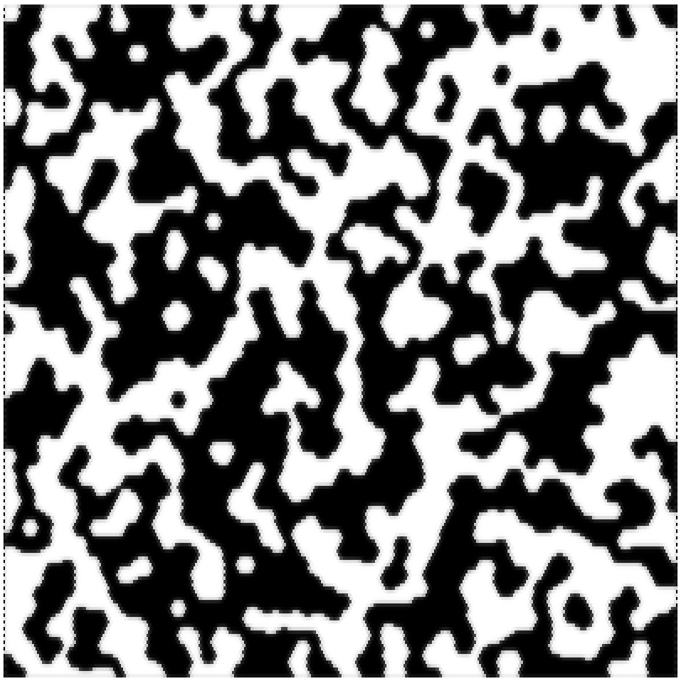

FIG. 1. Simulated ocular dominance patterns using only nearest neighbor interactions. Dark and light areas indicate strong preference for right or left eyes. Very little grey is apparent indicating few binocular cells. The domains do not form stripes with a regular width. In this simulation on a 200 x 200 lattice, $k_s = 0.125$, and $\Delta t = 0.05$. The simulation is interrupted when all $\Delta m_i/\Delta t$ are less then 10^{-10}. Due to an artifact of discretization, this pattern is metastable and does not coarsen to a single domain.

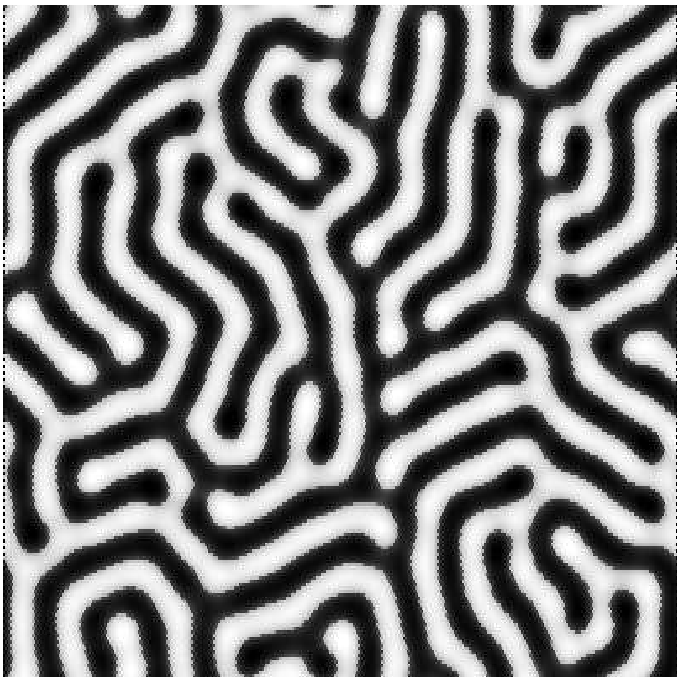

FIG. 2. Simulated ocular bands generated by iterating Eq. (7), with the fully isotropic interactions in Eq. (8). In this simulation on a 200 x 200 lattice, $k_s^{(2)} = 0.05$, $k_l^{(2)} = -0.025$, $\Delta t = 0.025$ and $L = 10$. The simulation is interrupted after 40 time constants when the mean value of $\Delta m/\Delta t$ is less than 0.01.

FIG. 3. Similar to Fig. (2), but with open boundary conditions which set $m_i = 0$ at the edges. Note that the bands now tend to meet the edges at right angles.

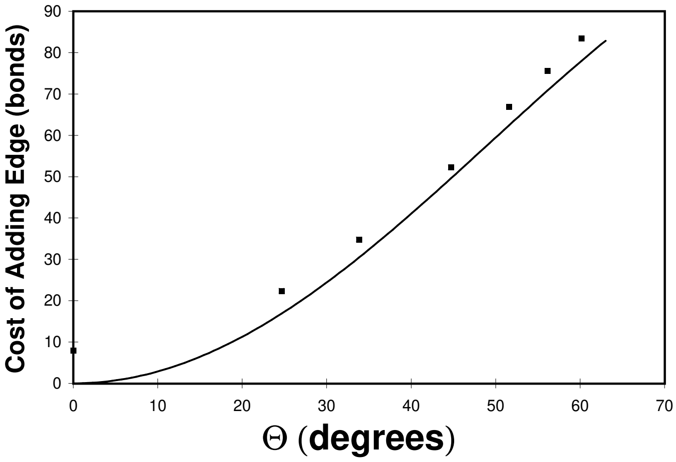

FIG. 4. The cost of stripes intersecting an edge at an angle θ to the normal, per unit length of the edge. The solid line is a calculation for a continuous system, while the dotted line is for a discrete model on a hexagonal lattice with a band width of 10 sites. In both cases the interaction occurs at the same range as the stripe width.

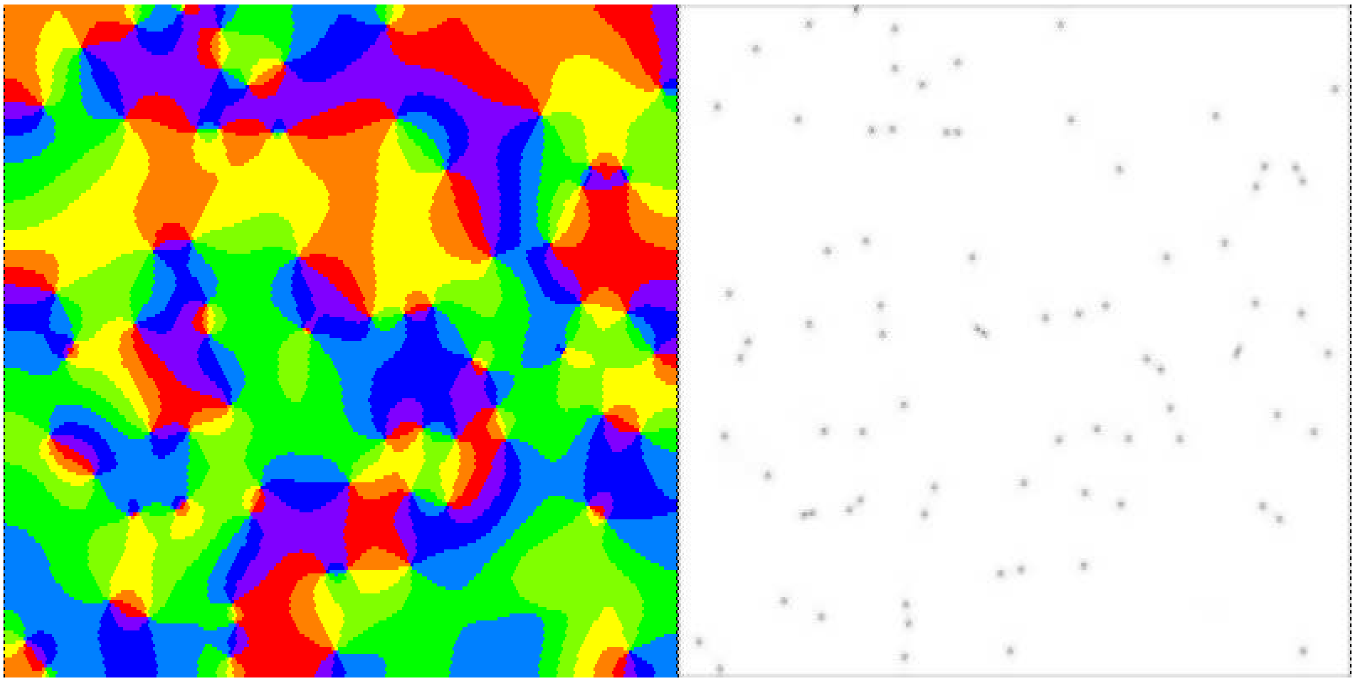

(a) (b)

FIG. 5. Simulated (a) orientation preference, and (b) selectivity, generated by iterating Eq. (16). In (a) each of the 8 colors shown represents a range of 45°. The colors cycle though 180° of preference as, light green → yellow → orange → red → violet → dark blue → light blue → dark green → light green → etc. In (b) darker areas are less selective. In this simulation on a 200 x 200 lattice, $k_s' = 0.125$ and $\Delta t = 0.05$. The simulation is interrupted after 50 time constants.

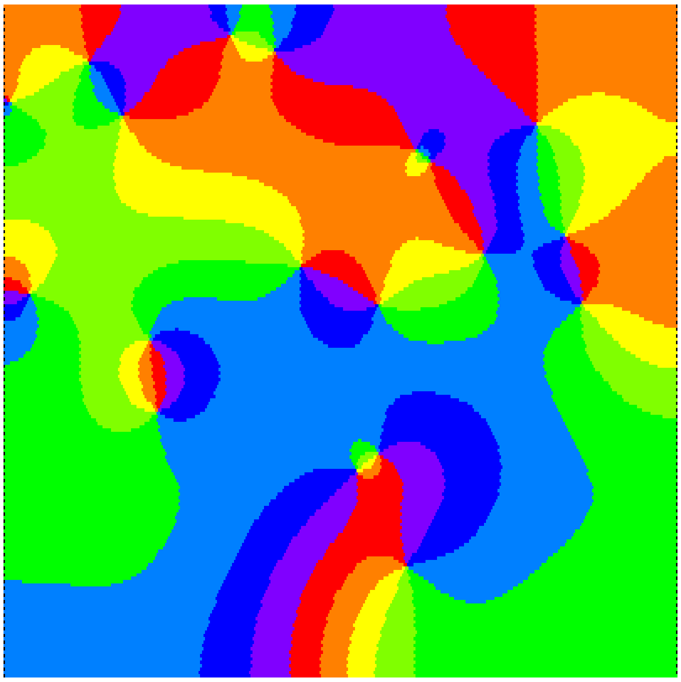

FIG. 6. The same simulated orientation pattern as in Fig. (5)a, but after 250 time constants. The number of vortices is greatly reduced. The remaining vortices eventually annihilate after additional iterations.

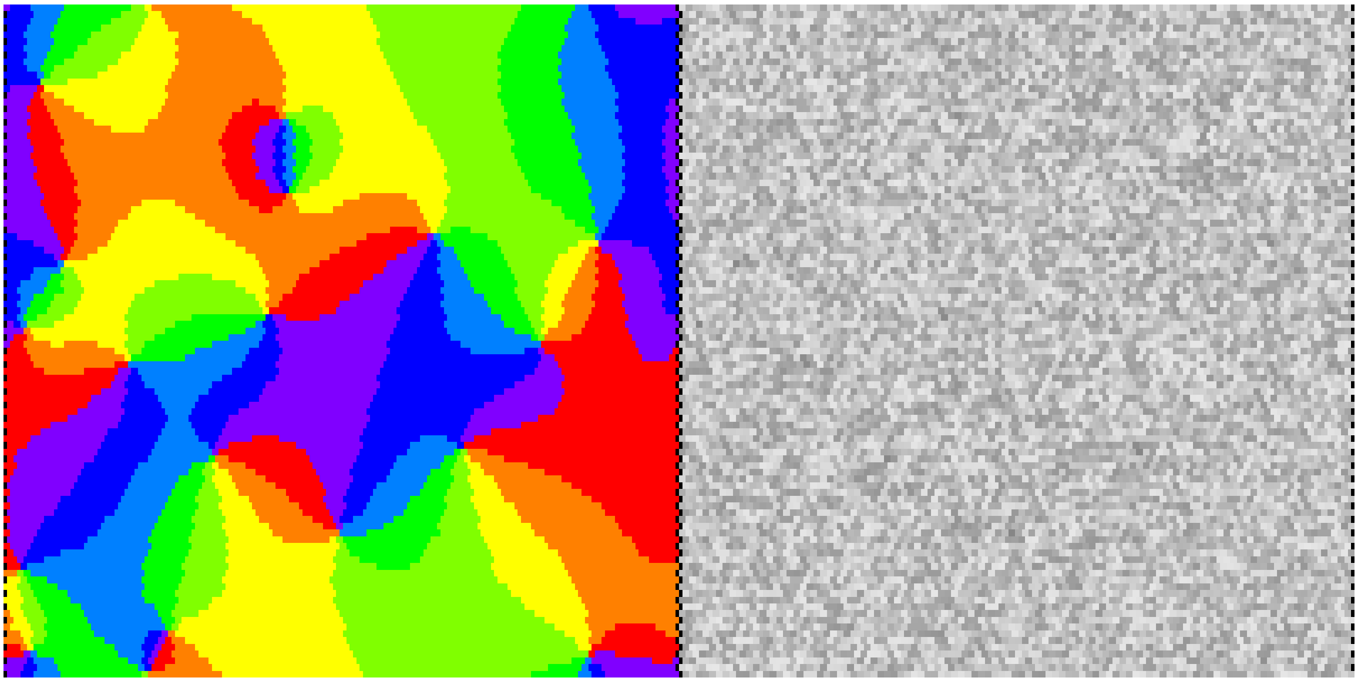

(a) (b)

FIG. 7. Simulated (a) orientation and (b) selectivity pattern generated by iterating Eq. (17). Here h_i' is distributed uniformly over the interval $(-2, 2)$. The randomness stabilizes the pattern of vortices but disrupts the pattern of selectivity. In this simulation on a 100 x 100 lattice, $k_s' = 0.05$, $\Delta t = 0.05$. The simulation is interrupted after 2500 time constants when the pattern appeared to be stable.

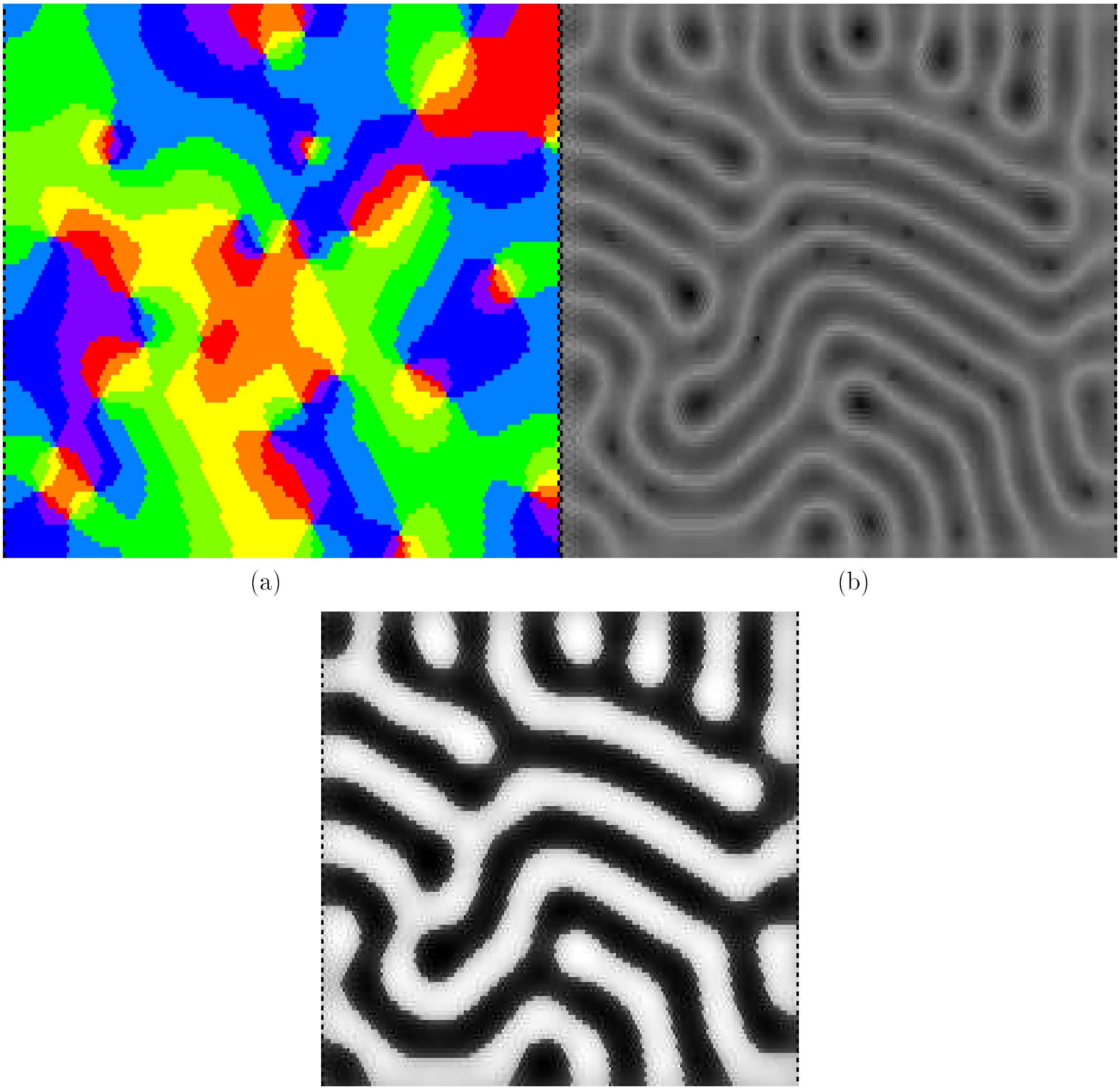

FIG. 8. Simulated (a) orientation preference, (b) orientation selectivity, and (c) ocular dominance patterns generated by iterating Eqs. (23). The coupling between fields prevents the further coarsening of defects. The locations of the vortices and ocular dominance domain walls are clearly visible in the orientation selectivity pattern. In this simulation on a 100x100 lattice, $\gamma = -0.1$, $k_s = -0.05$, $k_l = -0.025$, $L = 10$, $k'_s = 0.05$, and $\Delta t_m = \Delta t_z = 0.025$. The equations of motion were iterated for 500 time constants. The pattern appeared to be stable during the last 250 time constants.

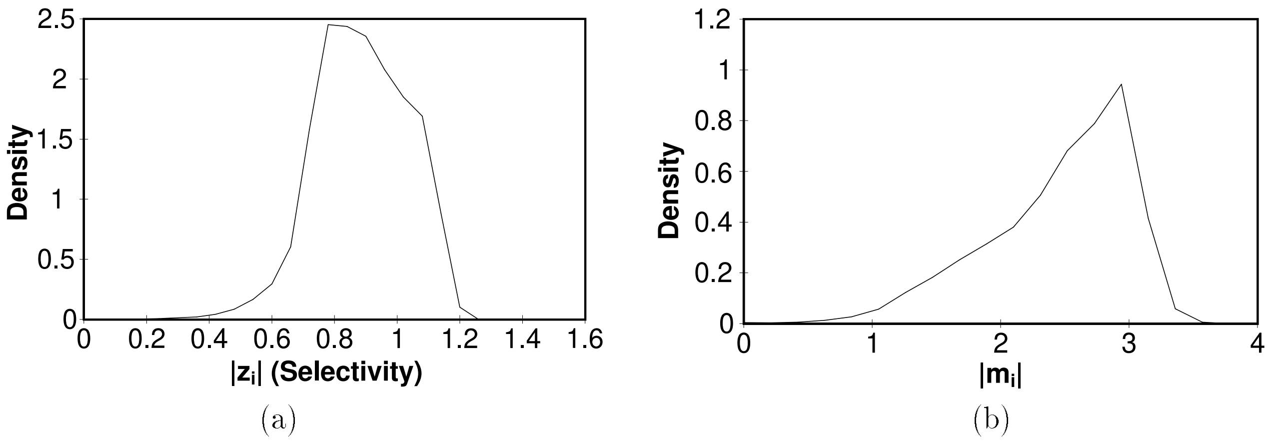

FIG. 9. The distributions of (a) $|z_i|$, and (b) $|m_i|$, corresponding to the patterns in Fig. (8).